Mecánica Computacional, Volumen XVIII - pp. 33-42
Compilado por: E. Dari, C. Padra y R. Saliba
San Carlos de Bariloche, noviembre de 1997

THE TWO-PHASE FLOW AROUND A SHIP

Pablo M. Carrica, Fabián J. Bonetto
Grupo Termohidráulica
Centro Atómico Bariloche and Instituto Balseiro
8400 - Bariloche, Argentina

Donald Drew
Department of Mathematical Sciences
Rensselaer Polytechnic Institute
Troy, NY 12180-3590, USA

RESUMEN

El objetivo de este trabajo es mostrar el progreso hecho en el modelado del flujo de dos fases burbujas/agua alrededor de un barco de superficie. Se discuten tres tipos de modelos de dos fluidos: de tamaño fijo, de tamaño variable monodisperso y polydisperso. Se presenta y discute brevemente el esquema numérico utilizado para resolver estos modelos, recalcando los puntos mas problemáticos. Se presentan algunos resultados para dos casos distintos.

ABSTRACT

The purpose of this paper is to report the progress made in the modeling of the bubbly two-phase flow around a surface ship. Three types of two-fluid models are discussed: single size model, variable size monodisperse and polydisperse. The numerical approach used to solve these models is presented and briefly discussed, remarking the weak points. Some results for two different cases are presented.

INTRODUCTION

The bubbly two-phase flow around a surface ship is attracting increasing attention, probably due to the fact that the numerical simulation of this problem has become feasible [1]. It is known that the presence of bubbles can have an effect on important design parameters such as ship drag, the wave fields and propeller performance. It is also known that the extent and characteristics of the two-phase wake are very important parameters to detect ships (and avoid detection), both from underwater and from satellites.

The sources of the bubbles that are present around a ship can be mainly two: the bubbles produced by the ship itself and the bubbles that are already in the ocean due to breaking and spilling waves and other aeration processes. Unfortunately the mechanisms involved in these bubble entrainment processes are far from being fully understood [2].

In this paper we present three two fluid models of increasing complexity for the calculation of the bubbly two-phase flow around a ship, and then we discuss the numerical methods involved in their resolution. Results are given for the cases of background ocean bubbles without bubble production by the ship, and for simulated ship-generated breaking waves. The geometry of a US naval combatant FF1052 was chosen to test the models [1]. The problems found in the numerical resolution of the resultant differential equations are discussed. Improvements in the modeling are proposed.

TWO-FLUID MODELS

The fundamental variable to describe bubbly flows is the bubble distribution function $f\left(\vec{\phi},\vec{r},t\right)$, defined so that the number of bubbles with internal variables in the range $\left(\vec{\phi},\ \vec{\phi}+d\vec{\phi}\right)$, located in a volume $d\vec{r}$ around a spatial location $\vec{r}$ at time t is $f\left(\vec{\phi},\vec{r},t\right) d\vec{r}\, d\vec{\phi}$. For the sake of simplicity, all the derivations will be made assuming that all the relevant internal variables can be calculated in some way from the bubble mass, so the bubble distribution function is described by the bubble mass, position and time. A similar approach, but using the bubble volume as internal variable, is frequently used in the theory of aerosols in which the gas is the continuous phase [3] and was

applied to incompressible bubbly two-phase flows [4,5]. By taking the mass moments of the distribution function we obtain the bubble number density N and the bubble mass density ε_m:

$$N(\vec{r},t) = \int_0^\infty f(m,\vec{r},t)\,dm \tag{1}$$

$$\varepsilon_m(\vec{r},t) = \int_0^\infty m\, f(m,\vec{r},t)\,dm \tag{2}$$

The gas volume fraction, or void fraction, can be calculated from the local mass density and the gas density. Assuming that the bubble velocity for a given size is known, we can write the conservation equation for the bubble size distribution function [4]:

$$\frac{\partial f}{\partial t} + \frac{\partial}{\partial x_j}\left[u_j\, f\right] + \frac{\partial}{\partial m}\left[\frac{d\,m}{d\,t} f\right] = \beta + \chi + S \tag{3}$$

where β is the net source due to bubble breakup, χ is the net bubble source due to coalescence and S is a bubble production term. The third term on the left-hand side is related to the mass change caused by dissolution of bubbles in the sea. This is an important term in our case. The modeling of the breakup and coalescence exchange terms for binary interactions is extensively explained in the references [3], [4] and [5] and will not be discussed here.

The numerical solution of Eq. (3) can be better found using a multigroup scheme, assuming that all the bubbles of mass between $m_{g-1/2}$ and $m_{g+1/2}$ can be represented in a group-g by a single bubble mass, m_g. We note that $m_{g-1/2}$ and $m_{g+1/2}$ must be chosen using some adequate criteria, such as good representation of the distribution, computational advantage, etc. Integrating Eq. (3) between $m_{g-1/2}$ and $m_{g+1/2}$ one obtains:

$$\frac{\partial N_g}{\partial t} + \frac{\partial j_{g,j}^N}{\partial x_j} + \left[\frac{d\,m}{d\,t} f\right]_{m_{g-1/2}}^{m_{g+1/2}} = \int_{m_{g-1/2}}^{m_{g+1/2}} \left[\beta + \chi + S\right] dm \tag{4}$$

where the bubble flux and number density in the group-g can be calculated as:

$$j_{g,j}^N = \int_{m_{g-1/2}}^{m_{g+1/2}} u_j(m,\vec{r},t)\, f(m,\vec{r},t)\, dm \tag{5}$$

$$N_g(\vec{r},t) = \int_{m_{g-1/2}}^{m_{g+1/2}} f(m,\vec{r},t)\, dm \tag{6}$$

As a further assumption, the distribution function, the bubble velocities, the bubble mass exchange rate and the breakup and coalescence probability are assumed constant in each group. Additionally, an upwinding approach is used to calculate the mass loss (or gain) rate in Eq. (4). Under these conditions Eq. (4) can be simplified to:

$$\begin{aligned}\frac{\partial N_g}{\partial t} + \frac{\partial\left(u_{g,j}\, N_g\right)}{\partial x_j} = {} & \beta_g^+ - \beta_g^- + \chi_g^+ - \chi_g^- + S_g - \frac{1}{m_{g+1} - m_g}\left[\min\left(\frac{d\,m}{d\,t},0\right) N\right]_{g+1} + \\ & \frac{1}{m_g - m_{g-1}}\left[\min\left(\frac{d\,m}{d\,t},0\right) N\right]_g - \frac{1}{m_{g+1} - m_g}\left[\max\left(\frac{d\,m}{d\,t},0\right) N\right]_g + \frac{1}{m_g - m_{g-1}}\left[\max\left(\frac{d\,m}{d\,t},0\right) N\right]_{g-1}\end{aligned} \tag{7}$$

The mass change rate in a bubble, dm/dt, is negative for the case of condensation or gas dissolution, and is positive in the case of evaporation or gas diffusion into the bubble. The bubble breakup, coalescence and volume sources and losses are also integrated over each group, resulting in the positive and negative terms on the right hand side of Eq. (7). The calculation of these terms requires the precise determination of the mass of each group. We can distinguish three cases:

(a) All the bubbles have the same mass m everywhere, in which case we have a single size model. In this case no breakup, coalescence or dissolution may occur, reducing Eq. (7) to:

$$\frac{\partial N}{\partial t} + \frac{\partial \left[u_{g,j} \; N \right]}{\partial x_j} = 0 \tag{8}$$

The void fraction can be calculated directly from the local number density.

(b) All the bubbles have the same local mass m, but this mass is a function of the position. In this case the system reduces to a system of two equations

$$\frac{\partial N}{\partial t} + \frac{\partial \left[u_{g,j} \; N \right]}{\partial x_j} = 0 \tag{9}$$

$$\frac{\partial \left(\rho_g \, \alpha \right)}{\partial t} + \frac{\partial \left(\rho_g \, \alpha \, u_{g,j} \right)}{\partial x_j} = \frac{dm}{dt} N \tag{10}$$

(c) The mass variable is discretized as necessary to resolve the bubble size distribution. This approach is called a multigroup approach. The multigroup can be defined with constant size groups [6] or with variable size groups following the characteristics lines determined by the dominating phenomenon, in our case dissolution. In our work we used the first approach, which imposes the resolution of one equation like Eq. (7) for each of the NG groups. In this case the bubble volume fraction is related to the group number density by:

$$\alpha\left(\vec{r} \, , t \right) = \sum_{g=1}^{NG} \frac{m_g \; N_g\left(\vec{r} \, , t \right)}{\rho_g\left(\vec{r} \, , t \right)} \tag{11}$$

These multigroup models can be solved in combination with a two-fluid model to calculate the gas velocity field for each group. Also, suitable models for bubble breakup, coalescence and dissolution are necessary to close the model. These models are presented in detail in reference [6].

The multigroup two-fluid model is derived based on the single group two-fluid model developed over the years at RPI [7,8,9,10] and by others [11,12]. The equation (7) corresponding to the model (a), (b) or (c) will be solved along with the momentum equations for the liquid and gaseous phases and the continuity equation for the liquid arising from the two-fluid model. The three dimensional two-fluid model can be written as:

$$\frac{\partial \alpha_k \, \rho_k}{\partial t} + \frac{\partial}{\partial x_j}\left(\alpha_k \, \rho_k \, u_{k,j} \right) = S_k \tag{12}$$

$$\frac{\partial \alpha_k \, \rho_k \, u_{k,i}}{\partial t} + \frac{\partial}{\partial x_j}\left(\alpha_k \, \rho_k \, u_{k,i} \, u_{k,j} \right) = \frac{\partial}{\partial x_j}\left[\alpha_k \left(\tau_{k,ij} + \tau_{k,ij}^{\mathrm{Re}} \right) \right] + M_{k,i} - \alpha_k \, \rho_k \, g \, \delta_{i3} \tag{13}$$

where $k = g$ or l denotes the gas group-g or the liquid phase, α_k is the phasic volume fraction at group-g, ρ_k is the phasic density, $u_{k,i}$ is the velocity of phase-k, $\tau_{k,ij}$ and $\tau_{k,ij}^{\mathrm{Re}}$ are the viscous stress tensor and the turbulent

stress tensor of phase-k, $M_{k,i}$ is the interfacial momentum transfer between the phases, and the last term on the right hand side of Eq. (13) is the gravitational force (In this work we use the piezometric pressure instead of the absolute pressure). Neglecting the mass transfer to the liquid, the mass conservation in the liquid yields:

$$\frac{\partial(\alpha_l \rho_l)}{\partial t} + \frac{\partial}{\partial x_j}\left(\alpha_l \rho_l u_{l,j}\right) = 0 \tag{14}$$

where the liquid density, ρ_l, is considered to be constant. Assuming also that the inertia and shear stress tensors are negligible for the gas phase, we can write the gas momentum equation for the group-g (g = 1, 2, ..., NG) as:

$$-\frac{\partial}{\partial x_i}\left(\alpha_g\ p\right) - \alpha_g\ \rho_g\ g\ \delta_{i3} + M_{g,i} = 0 \tag{15}$$

where the interfacial momentum transfer term for the liquid phase can be written as:

$$M_{l,i} = -\sum_{g=1}^{NG} M_{g,i} \tag{16}$$

Expanding the interfacial exchange terms we can write the gas momentum equation for group-g in the form:

$$-\frac{\partial\left(\alpha_g\ p\right)}{\partial x_i} - \alpha_g\ \rho_g\ g\ \delta_{i3} - p\frac{\partial\left(1-\alpha_g\right)}{\partial x_i} + M_{g,i}^{VM} + M_{g,i}^{L} + M_{g,i}^{D} + M_{g,i}^{TD} = 0 \tag{17}$$

where the source was separated into the virtual mass, lift, drag and turbulent dispersion force contributions. Details on the derivation of these forces are given in references [6] and [13]. The liquid momentum equation results then, combining Eqs. (13), (15) and (16):

$$\frac{\partial u_{l,i}}{\partial t} + u_{l,j}\frac{\partial u_{l,i}}{\partial x_j} + \frac{1}{\alpha_l}\frac{\partial}{\partial x_j}\left[\alpha_l\ \overline{u'_{l,i}\,u'_{l,j}}\right] =$$
$$-\frac{1}{\rho_l}\frac{\partial p}{\partial x_i} + \frac{\nu}{\alpha_l}\frac{\partial}{\partial x_j}\left[\alpha_l\left(\frac{\partial u_{l,i}}{\partial x_j} + \frac{\partial u_{l,j}}{\partial x_i}\right)\right] + \frac{\alpha_l\ \rho_l + (1-\alpha_l)\rho_g}{\alpha_l\ \rho_l} g\ \delta_{i3} \tag{18}$$

The Reynolds stresses were modeled using the Baldwing-Lomax [14] turbulence model. Replacing the definitions for the interfacial forces [6,13] and nondimensionalizing the system of equations with the ship length L and speed U_0 as nondimensionalization parameters, we obtain the final set of equations:

$$\frac{\partial \alpha_l}{\partial \hat{t}} + \frac{\partial\left[\alpha_l\ \hat{u}_{l,j}\right]}{\partial \hat{x}_j} = 0 \tag{19}$$

$$\frac{\partial \hat{N}_g}{\partial \hat{t}} + \frac{\partial\left(\hat{u}_{g,j}\ \hat{N}_g\right)}{\partial \hat{x}_j} + \frac{1}{\hat{m}_{g+1} - \hat{m}_g}\left[\min\left(\frac{d\,\hat{m}}{d\,\hat{t}},0\right)\hat{N}\right]_{g+1} - \frac{1}{\hat{m}_g - \hat{m}_{g-1}}\left[\min\left(\frac{d\,\hat{m}}{d\,\hat{t}},0\right)\hat{N}\right]_{g} +$$
$$\frac{1}{\hat{m}_{g+1} - \hat{m}_g}\left[\max\left(\frac{d\,\hat{m}}{d\,\hat{t}},0\right)\hat{N}\right]_{g} - \frac{1}{\hat{m}_g - \hat{m}_{g-1}}\left[\max\left(\frac{d\,\hat{m}}{d\,\hat{t}},0\right)\hat{N}\right]_{g-1} = \hat{\beta}_g^{+} - \hat{\beta}_g^{-} + \hat{\chi}_g^{+} - \hat{\chi}_g^{-} \tag{20}$$

$$\frac{\partial \hat{u}_{l,i}}{\partial \hat{t}} + \left[\hat{u}_{l,j} - \frac{1}{\alpha_l}\frac{\partial}{\partial \hat{x}_j}\left(\frac{\alpha_l}{\mathrm{Re}_l}\right)\right]\frac{\partial \hat{u}_{l,i}}{\partial \hat{x}_j} - \frac{1}{\alpha_l}\frac{\partial}{\partial \hat{x}_j}\left(\frac{\alpha_l}{\mathrm{Re}_l}\right)\frac{\partial \hat{u}_{l,j}}{\partial \hat{x}_i} =$$
$$-\frac{\partial}{\partial \hat{x}_i}\left(\hat{p} + \frac{2}{3}\hat{k}\right) + \frac{1}{\mathrm{Re}_l}\frac{\partial}{\partial \hat{x}_j}\left(\frac{\partial \hat{u}_{l,i}}{\partial \hat{x}_j} + \frac{\partial \hat{u}_{l,j}}{\partial \hat{x}_i}\right) + \frac{1-\alpha_l}{\alpha_l}\left[-\frac{\partial}{\partial \hat{x}_i}\left(\hat{p} + \frac{2}{3}\hat{k}\right) + \frac{1}{Fr^2}\right] \tag{21}$$

$$C_{vm}\left[\left(\frac{\partial \hat{u}_{g,i}}{\partial \hat{t}} + \hat{u}_{g,j}\frac{\partial \hat{u}_{g,i}}{\partial \hat{x}_j}\right) - \left(\frac{\partial \hat{u}_{l,i}}{\partial \hat{t}} + \hat{u}_{l,j}\frac{\partial \hat{u}_{l,i}}{\partial \hat{x}_j}\right)\right] = -C_L\,\varepsilon_{ijk}\,\varepsilon_{klm}\left(\hat{u}_{l,l} - \hat{u}_{g,l}\right)\frac{\partial \hat{u}_{l,l}}{\partial \hat{x}_m}$$
$$+\hat{C}_D\left(\hat{u}_{l,i} - \hat{u}_{g,i}\right)|\vec{u}_r| - \frac{\partial\left(\hat{p} + 2/3\hat{k}\right)}{\partial \hat{x}_i} + \frac{\delta_{i,3}}{Fr^2} - \hat{C}_D\,|u_r|\frac{\hat{\nu}_t}{Sc_b}\frac{1}{\hat{N}_g}\frac{\partial \hat{N}_g}{\partial \hat{x}_i} \tag{22}$$

Eqs. (19), (20), (21) and (22) are the mass and momentum conservation for the liquid and the bubbles of group-g. The resulting dimensionless parameters are the Reynolds and Froude numbers and the modified drag coefficient:

$$\mathrm{Re}_l = \frac{U_0\,L}{\nu_{eff}},\; Fr = \frac{U_0}{\sqrt{g\,L}},\; \hat{C}_D = \frac{3}{8}C_D\frac{L}{r_b} \tag{23}$$

NUMERICAL METHOD

The system of equations was solved using a transformation of coordinates from the physical domain into a computational domain with curvilinear coordinates. The transformation was chosen such that in the computational domain the computational cells are cubic with sides of unity length. To accommodate the flat transom stern of the ship, a two block approach was used, with bilinear interpolation between the corresponding faces of the blocks.

The group-g gas momentum equations were solved using a control volume full upwinding approach. As these equations are source dominated for small bubbles (algebraic if not for the virtual mass term), it is enough with this first order method. For the number density and, for models (a) and (b), the gas volume fraction equations, a TVD flux limiter was added to reduce the artificial diffusivity [15,16], then resulting in a second order accurate scheme. The 'superbee' compressive flux limiter function of Roe [15] was chosen. Complete details of the computational method are given in reference [13].

The liquid momentum and mass conservation equations were solved with the CFDSHIP-IOWA code developed by Tahara & Stern [17]and Stern et al. [18], in a modified form to account for the presence of gas bubbles, as shown in Eqs. (19) and (21). In this code the momentum equations are discretized using a 12-point finite-analytic method. The numerical method is modified due to the presence of several source terms arising from the interaction with gas and from the fact that now the liquid velocity field does not satisfy zero divergence. Additionally, the presence of the liquid volume fraction is now multiplying the stress tensors. CFDSHIP-IOWA uses the pressure-implicit split-operator (PISO) algorithm to make the method equal-order. The liquid continuity equation is solved in a control volume and the liquid volume fraction is included to calculate the mass fluxes through the walls of the cell.

The solution procedure for the liquid equations using the PISO algorithm is as follows: first, the momentum equations are solved implicitly using the pressure from the previous time step. Second, the pressure equation is solved implicitly to obtain an intermediate pressure, and the corrected velocity field is solved explicitly to satisfy the continuity equation and the pressure is recalculated. Since in this work we are calculating steady-state flows, the velocity and pressure fields do not have to be completely converged at each "time step", thereby allowing a more economical way to reach steady-state by making a few iterations of the pressure and momentum equations at each time step. The same principle is applied when solving the equations for the gas phase. Finally, all the

equations are solved using a tridiagonal solver and the method of lines. For further details on the numerical method the reader should see the references cited.

Referring to Fig. 1, the solution domain extends from x/*L*=-0.4 to x/*L*=2 and up to a radial distance from the axis r/*L*=1. As the case is symmetrical respect to the centerplane, only half of the domain must be calculated. The grid extends in the computational domain in the ξ (as x), η (from the hull towards the outer boundary) and ζ (from the centerplane to the free surface) directions in H-grid topology. Cuts of the grid are shown in Fig. 1. Two cases are presented for the FF-1052 US Navy frigate, which is *L*=126.7 *m* long with a transom stern and a bulbous bow to accommodate a sonar dome. In both cases the ship was unpropelled. The speed used for calculations was 27 knots (13.5 *m/s*), which results in full-scale Reynolds and Froude numbers of Re=1.7x10^9 and Fr=0.39. In case 1 we used model (b) for Re=1x10^6 and Fr=0.39 and full-scale bubble parameters with the following boundary conditions: at the liquid entrance, x/*L*= -0.4, $u_l = u_g = 1, v_l = v_g = 0, w_l = w_g = 0, \frac{\partial p}{\partial x} = 0$ and a sheet of bubbles enters the domain with average size of 75 micrometers and with a distribution z^{-3} starting with 5 % at the sea level, as measured in reference [2] for background sea bubbles; at the exit, x/*L* = 2, $\frac{\partial u_l}{\partial x} = \frac{\partial v_l}{\partial x} = \frac{\partial w_l}{\partial x} = \frac{\partial p}{\partial x} = 0$; at the hull, non-slip conditions for the liquid velocity; at the centerplane, zero pressure and liquid velocity gradients; at the outer boundary, $u_l = 1, v_l = 0, p = 0$ and w_l is calculated from liquid continuity, and the gas is free to leave the domain; at the free-surface, the bubbles are free to leave the control volume. The turbulent dispersion is set to zero to avoid unrealistic loss of bubbles or entrance of air. For the liquid the model of Stern et al. [18] was used, where an exact nonlinear free-surface cinematic equation and an approximate dynamic free-surface condition were solved. For details about the solution method for the free surface equations the reader is referred to the work of Stern et al. [18].

In case 2 the conditions are essentially the same as in case 1, except that no bubbles are present in the background sea and at the free surface the boundary conditions are zero Fr number (flat surface) and a simulated liquid and gas breaking wave is located between x/*L*=2.7x10^{-3} and x/*L*=2.9x10^{-2} and from 0.4 *m* to 1.7 *m* from the hull, entering with a vertical velocity -2.7 *m/s* and with 10 % gas volume fraction. The bubble size distribution used was that measured by Cartmill and Su [19], who studied the bubble radius distribution for a breaking wave in salt water from 34 *μm* to 1200 *μm*. Fifteen (15) size groups were used with bubble radius at normal pressure between 10 *μm* and 1000 *μm*. Case 2 was solved using method (c).

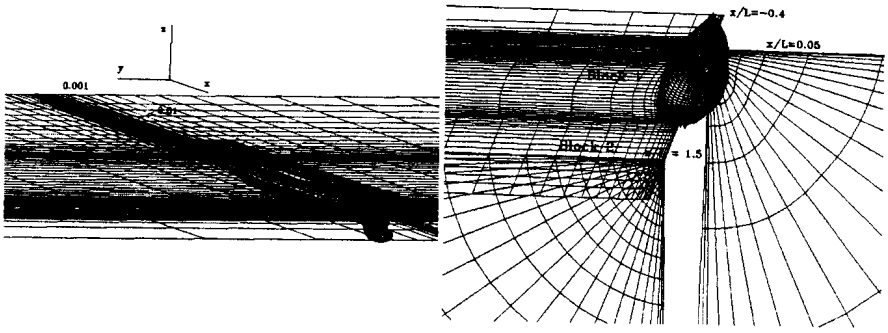

Figure 1: FF1052 geometry and gas volume fraction at the free surface for case 2 (left). Computational grid and block disposition (right).

To study grid convergence, four grids where used for case 1, with 78x21x22 (very coarse), 110x21x22 (coarse), 110x31x22 (medium) and 110x40x40 (fine) nodes in the ξ, η and ζ directions. The first row of nodes is located within $y^+<2$, in accordance to the Baldwin-Lomax turbulence model requirements. For case 2, with Fr=0, the numerical solution of the problem is heavier with 15 groups, so only the very coarse grid was used no grid convergence was tested.

The equations were solved iteratively using a pseudo-transient marching process in the x-direction and the method of lines at each perpendicular plane. The convergence was evaluated measuring the L_2 norm of the different independent variables. One variable was considered converged when the decrease in the L_2 norm was more than three orders of magnitude. To achieve convergence, it was necessary to overrelax the gas momentum equations with increasing relaxation constants up to about $1x10^{-4}$ in the last iterations. The convergence problems arise because of the presence of the number density gradients in the gas momentum equations Eq. (22) (turbulent dispersion term).

SOME RESULTS

In Fig. 2 (left) a comparison of the shape of the free surface is shown for the different grids used in case 1, for a case with $Re=4x10^6$ [18] and for data from an experiment at $Re=2x10^7$ [20]. It is known that the minimum at x/L about 0.6 decreases when the Re increases, and that is the trend shown in the calculations. It can be seen that the very coarse grid fails to follow the shape of the free surface. All the other grids converge to the same free surface form within 0.1 % total difference. The same can be said of the other variables involved in the problem. However, the grid convergence analysis performed is not conclusive, because of the impossibility of testing larger grids that could be necessary to calculate drag and other integrated parameters depending on the velocity gradients.

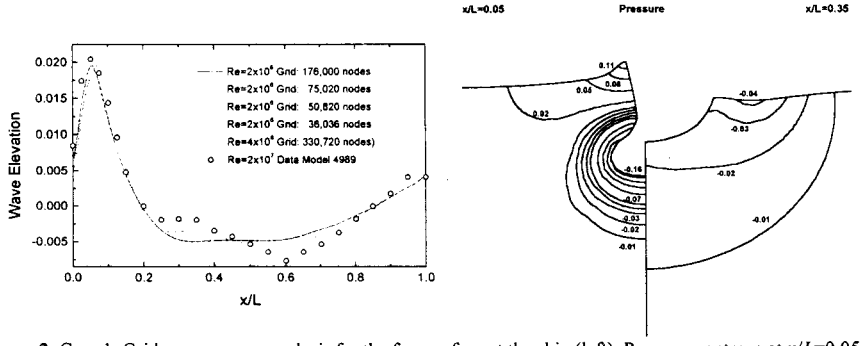

Figure 2: Case 1. Grid convergence analysis for the free surface at the ship (left). Pressure contours at x/L=0.05 and 0.35 (right)

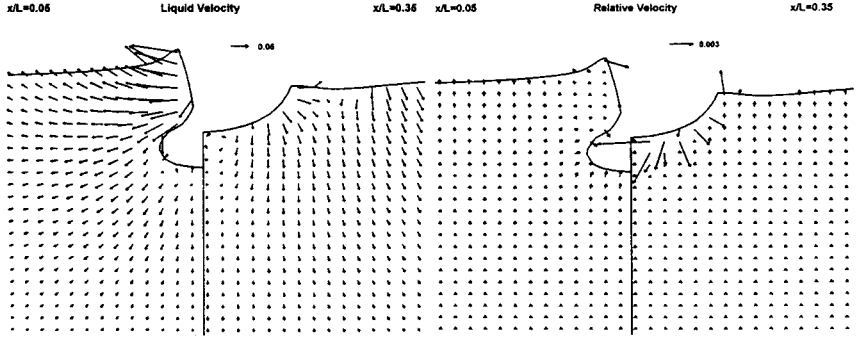

Figure 3: Case 1 at x/L=0.05 and 0.35. Transversal liquid velocity (left) and relative velocity (right).

Fig. 2 (right), Fig. 3 and Fig. 4 show pressure contours, transversal liquid velocity and relative velocity vectors and gas volume fraction and bubble average radius for x/L=0.05 and 0.35 stations. Figure 5 shows gas volume fraction and bubble average radius for x/L=0.65 and 0.95 stations. As the figures show, the ship has a strong effect on the bubble trajectory, modifying the relative velocity (see Fig. 3 right) in the near hull region mainly

due to lift and turbulent dispersion forces. This, combined with gravity, causes an accumulation of bubbles at the bottom of the hull, as is depicted in Figs. 4 and 5. On the other hand, the lower velocity in the ship boundary layer causes a higher transit time for the bubbles that are trapped by the hull, causing a smaller average radius in this region by increased dissolution effect.

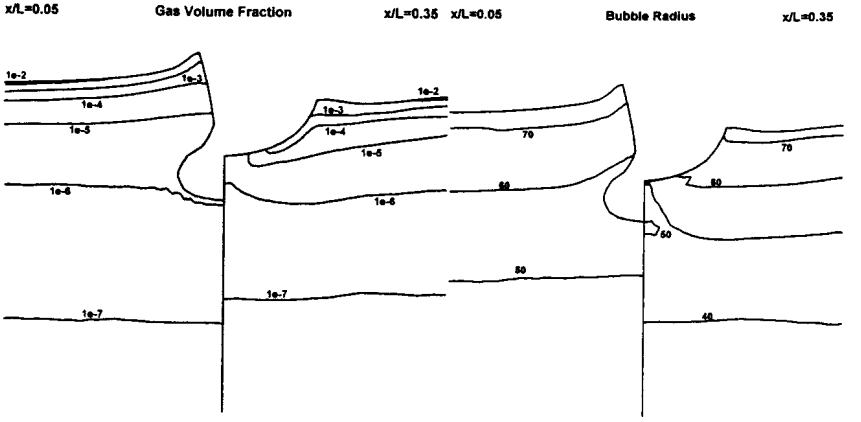

Figure 4: Case 1 at x/*L*=0.05 and 0.35. Gas volume fraction (left) and bubble average radius (right).

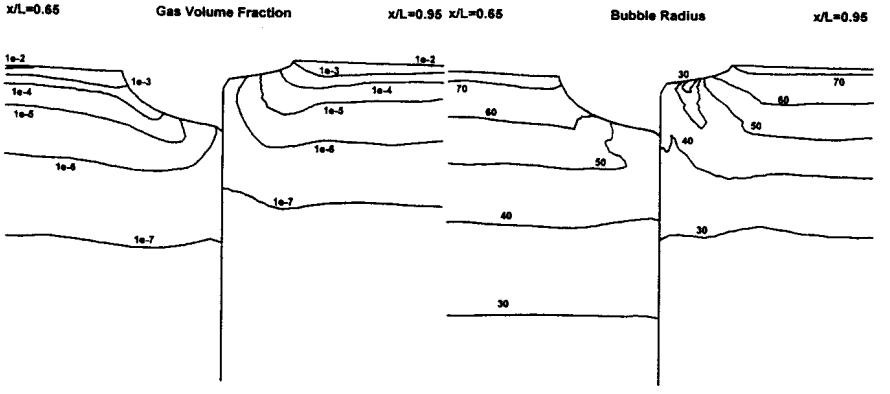

Figure 4: Case 1 at x/*L*=0.65 and 0.95. Gas volume fraction (left) and bubble average radius (μm) (right).

The results of case 2 are more difficult to analyze because of the large amount of information involved in this problem, and only a highlight of the trends will be shown. In Fig. 1 the gas volume fraction distribution at the sea level is shown. The injected bubbles at the bow form a bubbly wake that extends several ship lengths after the stern. Fig. 6 left shows bubble size distributions at the hull in x/*L*=0.95, 25 *cm* below the water surface, under different intergroup transfer mechanisms. Runs with only coalescence, breakup or dissolution were run and are shown in the figure, along with the results of the distribution without any intergroup source and with all the sources. A small peak can be observed at sizes below 100 μm, due to big bubbles that break into very small ones, effect caused by the strong velocity gradient present at the hull (tipstreming). Also, when breakup is present, a large transfer of gas from big bubbles to midsize bubbles (about 500 μm) can be observed. The effect of coalescence is the opposite but weaker. Dissolution is more difficult to analyze, because it causes an effective loss of gas mass, and as a consequence modifies the trajectory of the bubbles (smaller bubbles rise slower), then causing probably an accumulation of slightly smaller bubbles than in the case with no source.

Figure 6 right shows a comparison of the normalized distribution functions at the wake (x/L = 1.5, y/L = 0.04, z = 0, –2.15, -6 *m*) and at the hull, plus the reference distribution which is the bubble distribution size at the air entrainment location near the bow of the ship. Big bubbles are much more important in the near hull region, while at the wake we find more smaller bubbles as we go deeper (the big bubbles were already accumulated at the hull). The void fraction-weighted average radius decreases from about 550 μm at sea level to about 175 μm only 6 *m* below. This is partly due to pressure effects, but mainly because dissolution is stronger for smaller bubbles.

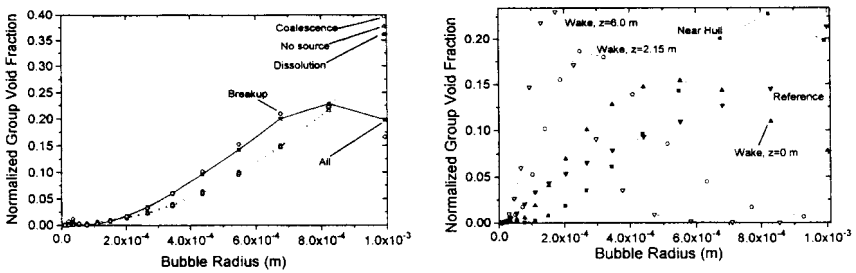

Figure 6: Case 2. Bubble size distributions at the near-hull location in x/L=0.95 with different various exchange sources considered (left) and comparison of bubble size distributions given by the full model at different locations (right).

CONCLUSIONS AND FURTHER WORK

As the calculation of complex three dimensional two-phase flow problems is becoming feasible from the computer technology standpoint, computational methods and physical models still need improvements. The main points that need work to allow us to use the word 'prediction' in polydisperse three dimensional bubbly flows are:

- Breakup, dissolution and coalescence models are neither accurate nor general enough to predict mass transfer rates between bubble sizes in general flows.
- Turbulence modeling of bubbly flows needs improvement to predict both the effects of the bubbles in the turbulent flow and of the turbulence into the bubble dispersion. Also the numerical implementation of the turbulent dispersion force is a problem.
- Most of the models for the interfacial forces available for the two-fluid model are valid only for small gas volume fraction, say less than 1 %. That is not true for many regions near the hull of the ship. It is necessary the development of models or corrections for high bubble concentrations.

Further work in the area includes the inclusion of propellers, both as sources of bubbles (because of cavitation) and as body forces in the flow, two-phase flow turbulence modeling, and generalization of the multi-block scheme to general geometry.

In spite of these drawbacks, the results presented in this paper show that at the present it is possible to estimate the two-phase flow field in complex three-dimensional problems.

ACKNOWLEDGEMENTS

This work was partially funded by the US Office of Naval Research under Grants N00014-91-J-1271 and N00014-96-1-0479. Most of the calculations were computed at the Naval Oceanographic Supercomputer Center on the Cray C90.

REFERENCES

[1] **E. Paterson, M. Hyman, F. Stern, P. M. Carrica, F. Bonetto, D. Drew & R. T. Lahey, Jr.** *Near and Far-Field CFD for a Naval Combatant Including Thermal-Stratification and Two-Fluid Modeling*, proc. 21st Symp. on Naval Hydrodynamics, Trondheim, Norway, 1996.

[2] **W. K. Melville, E. Terrill & L. Ding**, *Field Measurements of Air Entrainment by Breaking Waves*, in Air-Water Gas Transfer, AEON Verlag & Studio, 63454 Hanau, 1996.

[3] **M. M. R. Williams & S. K. Loyalka**, *Aerosol Science Theory and Practice*, Pergamon Press, Oxford, 1991.

[4] **G. Guido Lavalle, P. M. Carrica, A. Clausse & M. K. Qazi**, *A Bubble Number Density Constitutive Equation*, Nuclear Eng. Des. **152**, p. 213, 1994.

[5] **D. Sanz, G. Guido Lavalle, P. M. Carrica & A. Clausse**, *About the Statistical Description of Gas-Liquid Flows*, Proc. 7th International Meeting on Nuclear Reactor Thermal-Hydraulics, Saratoga Springs, USA, 1995.

[6] **P. M. Carrica, F. Bonetto, D. Drew & R. T. Lahey**, *A Polydisperse Model for Bubbly Two-Phase Flow Around a Surface Ship*, submitted to Int. J. Multiphase Flow, 1996.

[7] **D. Drew & R. T Lahey**, *Application of General Constitutive Principles to the Derivation of Multidimensional Two-Phase Flow Equations*, Int. J. Multiphase Flow **5**, p. 243, 1979.

[8] **G. Arnold**, *Entropy and Objectivity as Constraints Upon Constitutive Equations for Two-Fluid Modeling of Multiphase Flow*, Ph.D. Thesis, RPI, Troy, NY, USA, 1988.

[9] **J. W. Park**, *Void Wave Propagation in Two-Phase Flow*, Ph.D. Thesis, Rensselaer Polytechnic Institute, Troy, NY, USA, 1992.

[10] **A. Alajbegovic**, *Phase Distribution and Turbulence Structure for Solid/Fluid Upflow in a Pipe*, Ph.D. Thesis, Rensselaer Polytechnic Institute (RPI), Troy, NY, USA, 1994.

[11] **J. M. Delhaye**, See chapters 5, 7, 8 and 9 *in Thermohydraulics of Two-Phase Systems for Industrial Design and Nuclear Engineering*, Hemisphere Publishing Corp., New York, 1981.

[12] **M. Ishii**, *Thermo-Fluid Dynamic Theory of Two-Phase Flow*, Eyrolles, Paris, 1975.

[13] **P. M. Carrica, F. Bonetto, D. Drew & R. T. Lahey**, *The Interaction of Background Ocean Air Bubbles with a Surface Ship*, submitted to Int. J. Num. Meth. Fluids, 1996.

[14] **B. Baldwin & H. Lomax**, *Thin Layer Approximation and Algebraic Model for Separated Turbulent Flow*, AIAA 16th Aerospace Sciences Meeting, AIAA paper 78-257, 1978.

[15] **P. Roe**, *Some Contributions to the Modeling of Discontinuous Flows*, in Large-Scale Computations in Fluid Mechanics, AMS, Providence, RI, USA, 1985.

[16] **P. K. Sweby**, *High Resolution TVD Schemes Using Flux Limiters*, in Large-Scale Computations in Fluid Mechanics, AMS, Providence, RI, USA, 1985

[17] **Y. Tahara, F. Stern & B. Rosen**, *An Interactive Approach for Calculating Ship Boundary Layers and Wakes for Nonzero Froude Number*, J. of Comp. Phys. **98**, p. 33, 1992.

[18] **F. Stern, E. Paterson & Y. Tahara**, *CFDSHIP-IOWA: Computational Fluid Dynamics Method for Surface-Ship Boundary Layers and Wake and Wave Fields*, Iowa Institute of Hydraulic Research Report 666, Iowa City, USA, 1996.

[19] **J. W. Cartmill & Y. M. Su**, *Bubble Size Distribution Under Saltwater and Freshwater Breaking Waves*, Dynamics Atmos. Oceans **20**, p. 25, 1993.

[20] **T. Rattcliffe & W. T. Lindenmuth**, *Kelvin-Wake Measurements Obtained on Five Surface Ship Models*, DTRC-89/038, US Navy report 1990.